A new role of the lower hybrid drift instability in magnetic reconnection

Paolo Ricci*

Department of Physics and Astronomy,

Dartmouth College, Hanover NH 03755

J.U. Brackbill†

ParticleSolutions, Portland OR 97214

W. Daughton‡

University of Iowa, Iowa City

Giovanni Lapenta§

Istituto Nazionale per la Fisica della Materia (INFM),

Unità del Politecnico di Torino, Corso Duca degli Abruzzi 24 - 10129 Torino,

Italy and Los Alamos National Laboratory, Los Alamos NM 87545

(Dated: January 18, 2005)

Abstract

Kinetic simulation results reveal that the growth of the lower hybrid drift instability (LHDI) in current sheets has an important effect on the onset and non-linear development of magnetic reconnection. The LHDI does this by heating electrons anisotropically, by increasing the peak current density, by producing current bifurcation, and by causing ion velocity shear. The role of these in magnetic reconnection is explained. Confidence in the results is strongly enhanced by agreement between implicit and massively-parallel-explicit particle-in-cell (PIC) simulations.

*Electronic address: paolo.ricci@dartmouth.edu

†Electronic address: jerrybrackbill@comcast.net

‡Electronic address: william-daughton@uiowa.edu

§Electronic address: lapenta@lanl.gov

I. INTRODUCTION

The importance of the lower hybrid drift instability (LHDI) in the evolution of current sheets with thickness comparable to the thermal ion gyroradius has been studied for decades. The topic is of central relevance to the physics of magnetic reconnection and has widespread application to space, astrophysical and laboratory plasmas [1]. Early work on LHDI by Krall and Liewer [2] has been followed by numerous papers (see Ref. [1] for a review of the literature).

The LHDI is driven by the diamagnetic current that arises because of the presence of inhomogeneities in the density and magnetic field in a current sheet. The fastest growing modes are primarily electrostatic, and are confined to the edge region with $k\rho_e \sim 1$, $\omega \sim kU_i \leq \Omega_{lh}$, $\gamma \leq \Omega_{lh}$, where ρ_e is the electron gyroradius, U_i the ion diamagnetic drift velocity, $\Omega_{lh} \approx \sqrt{\Omega_{ce}\Omega_{ci}}$ is the lower-hybrid drift frequency (Ω_{ce} and Ω_{ci} are the electron and the ion gyrofrequencies, respectively) [3]. Longer wavelength modes, $k\sqrt{\rho_i\rho_e} \sim 1$ show a slower growth rate, $\gamma \sim \Omega_{ci}$, and have a significant electromagnetic component that can penetrate into the control region for sufficiently thin current layers [4].

Since it is a relatively short wavelength and high frequency instability, the LHDI has been considered for some years a source of anomalous resistivity, and it is often invoked to explain the discrepancy between the rapid observed rate of reconnection and the slow, theoretically predicted rate based on classical resistivity [5, 6]. Indeed the LHDI has been observed during magnetic reconnection in the magnetotail [7], in the magnetopause [8], and in laboratory experiments [10]. However, two problems make the explanation based on LHDI difficult to accept. First, both simulations [9] and observations [7, 10] show that the saturation level of the LHDI is determined primarily by the electron dynamics, and it is far too low to justify the anomalous resistivity that is required to obtain realistic reconnection rates. Second, the LHDI is mostly stabilized at high plasma β and thus it grows primarily on the flanks of the current sheet [11], unless the current layer is very thin [4].

Recently, the effects of the LHDI have been revisited [12–18]. In the present paper, it is shown that the LHDI has an important role in magnetic reconnection, but through a mechanism very different in nature than anomalous resistivity. Although the LHDI is a microscopic instability, it is responsible for macroscopic effects on the current sheet. The LHDI heats electrons anisotropically, preferentially in the perpendicular direction, peaks

and bifurcates the current sheet, and causes ion velocity shear [14, 15]. These effects have important consequences both on reconnection onset and on the non-linear development of reconnection. In particular, simulation results show that both temperature anisotropy with $T_{e\perp}/T_{e||} > 1$ and current peaking strongly enhance the linear growth rate of the tearing instability [14].

The paper reviews published results and introduces some new results on the scaling of LHDI evolution with the current sheet thickness. The scaling enables us to show that the effect of the LHDI decreases with the thickness of the current sheet profile, passing from current peaking to current bifurcation. Moreover, it is shown that the level of the electron anisotropy induced by the LHDI is reduced for thicker current sheets.

The paper is organized as follow. Sect. II describes the system we study and the simulation tools we use for the task. Sect. III focuses on the macroscopic effects of the LHDI, which are explained by a simple physical model in Sect. IV. Section V reviews results on the effect of the LHDI on the linear and nonlinear evolution of the tearing instability.

II. PHYSICAL SYSTEM AND THE SIMULATION APPROACH

Following the Geospace Environment Modelling (GEM) magnetic reconnection challenge [19], a Harris current sheet is considered [20]. The usual magnetotail reference frame is used, with the magnetic field aligned to the x direction,

$$\mathbf{B} = B_0 \tanh(z/L)\mathbf{e}_x \tag{1}$$

and plasma density given by

$$n = n_0 \mathrm{sech}^2(z/L) \tag{2}$$

The current sheet parameters are: $\omega_{pe}/\Omega_{ce} = 2.88$, $T_i/T_e = 5$, $m_i/m_e = 180$, and three different current sheet thicknesses are considered, $\rho_i/L = 1.828$, 0.915, and 0.457 ($v_{th,s} = \sqrt{2T_s/m_s}$). The boundary conditions are periodic in the x and y direction for both particles and fields. Conducting boundaries are imposed for the fields at the z boundaries, and reflecting boundary conditions are used for the particles. The domain considered is $L_y \times L_z = 12L \times 12L$.

To investigate the evolution of the system, a linear Vlasov code and two different nonlinear particle-in-cell (PIC) simulation codes are used. The linear Vlasov results use the formally exact approach described in Refs. [4] and [21]. This technique employs a normal mode calculation using a full Vlasov description for both ions and electrons. The orbit integrals arising from the linear Vlasov theory are treated numerically using the exact unperturbed particle orbits and including the form of the perturbation inside the integral. Both electromagnetic and electrostatic contributions to the field perturbation are retained and resulting system of integrodifferential equations is solved using a finite element expansion of the eigenfunction [4].

The nonlinear dynamics are simulated by two PIC codes, an explicit simulation code NPIC, and an implicit simulation code CELESTE3D. The explicit plasma simulation code NPIC is based on a well-known explicit electromagnetic algorithm [22, 23]. The particle trajectories within NPIC are advanced using the leapfrog technique, and particle moments are accumulated with area weighting. The simulations are run on a massively-parallel computer. The implicit plasma simulation code, CELESTE3D [24–26], solves the full set of Maxwell-Vlasov equations using the implicit moment method. Both Maxwells and Newtons equations are discretized implicitly in time. The implicit simulations are run on a workstation.

The nonlinear simulations are performed by the two codes with very different simulation parameters, as pointed out in Ref. [14].

III. NONLINEAR EVOLUTION OF THE LHDI

Simulations are performed in the (y, z) plane of the Harris current sheet, with several current sheet thicknesses. The initial Harris equilibrium is unstable to the LHDI and the early dynamics is dominated by this instability. In the present paper the focus is on the nonlinear consequences of the LHDI.

The LHDI modifies the current profile. In Fig. 1 the y-averaged current profile for the three current sheets thicknesses is represented after the growth of the LHDI.

For the thinnest case, $\rho_i/L = 1.828$, the LHDI causes a peaking of the current profile. This effect has been documented in previous works [12–14, 16–18, 27] and the alteration is primary due to electron acceleration: the ion and electron density modifications are weaker

[12, 13, 16**?**]. At a later stage in the evolution of the current sheet, a strong kink instability dominates the evolution of the current sheet [16–18]. Simulations have revealed that the current profile becomes bifurcated at this stage [28].

In the simulation of the current sheet with intermediate thickness, both NPIC and CELESTE3D show bifurcation of the current. Current bifurcation has been observed in satellite measurements of thin ($L \sim \rho_i$) [29] and thick current sheets ($L > \rho_i$) [30, 31], and in magnetic experiment [32]. The build-up of the bifurcated current sheet as a result of the LHDI was also recently shown in particle simulations by Sitnov *et al.* [33], starting from a non-Harris current sheet equilibrium. It should be remarked that current sheet bifurcation has also been explained as a consequence of the kink that affects the dynamics of the current sheets [34] or as a consequence of the physics in the reconnection plane [35, 36].

For the thickest current sheet, the agreement between NPIC and CELESTE3D is less good, mostly on the flanks of the current sheet, where CELESTE3D shows higher fluctuations in the current density than NPIC. Nevertheless, both codes reveal the same trends: no significative changes of the current density occur at the center of the current sheet and, in general, the changes in the current profile are less visible than in the cases of thinner current sheets. This shows that the effect of the LHDI decreases with the current sheet thickness.

The non-linear evolution of the LHDI not only heats electrons (an effect documented in many previous works, e.g., Ref. [9]) but preferentially heats electrons in the direction perpendicular to the magnetic field. The ratio of perpendicular to parallel electron temperature, $T_{e\perp}/T_{e||}$, from NPIC is shown in Fig. 2. The electron distribution functions are not gyrotropic in the thinnest current sheet case and the anisotropy decreases with the thickness of the current sheet. The values of anisotropy at the center of the current sheet from NPIC and CELESTE3D are listed in Table I.

Finally, the LHDI creates velocity shear. This latter consequence has been the subject of a number of papers (see Ref. [16] and references therein). Its main effect is to promote the growth of a Kelvin-Helmholtz instability (KHI), and three dimensional simulations show that the KHI appear to have an important effect on reconnection onset in the presence of a normal magnetic field B_z [16]. We note that at high mass ratio, the creation of a velocity shear due to LHDI and the subsequent KHI has been revealed by CELESTE3D, NPIC, and Hesse's code, while Pritchett's code has not shown the formation of a velocity shear. At low

mass ratio, current sheets are affected by a drift-kink instability that is stable at high mass ratio, whose consequences are similar to the ones due to the KHI.

[DO YOU KNOW THE REFERENCES FOR THE WORK BY PRITCHETT and HESSE? WOULD YOU PUT ANYTHING MORE HERE? MAYBE THE REFEREE WANT TO SEE MORE...]

IV. A SIMPLE PHYSICAL EXPLANATION

A simple physical model is sufficient to explain the consequences of the LHDI. We refer the reader to Refs. [15] and [17] for a complete description of the process, and in the following we summarize the basic mechanism. Particles can be distinguished between *crossing*, with trajectories that traverse both sides of the current layer, and *noncrossing* with trajectories that are confined to one side of the layer. The perpendicular kinetic energy $\epsilon = m_s(v_z^2+v_y^2)/2$ and canonical momentum $p_y = m_s v_y + q_s A_y/c$ ($A_y = -B_0 L \ln[\cosh(z,L)]$ in a Harris sheet) are constants of the particle motion, and only particles with $\epsilon > p_y^2/2m_s$ can cross the layer. The boundary between crossing and non-crossing particles can also be written as

$$\frac{v_y}{v_{th,s}} = \frac{\alpha}{2} - \frac{1}{2\alpha}\left(\frac{v_z}{v_{th,s}}\right)^2, \tag{3}$$

where $\alpha = (L/\rho_s)\ln[\cosh(z/L)]$. The approximate phase velocity of the LHDI for cold electrons is $\omega/k_y \approx U_i/2$ and it is in the proper region to permit resonant scattering of ions from crossing trajectories to non-crossing trajectories and *vice versa*. As it is shown in Fig.3, because of the slope of the distribution function in the vicinity of the resonance, the scattering from the crossing to the non-crossing region is more frequent. It should be remarked that scattering can only occur if the ion meandering length $\sqrt{2\rho_i L}$, which measures the spatial extent of the crossing ion orbits, overlaps with the localization of the LHDI.

Scattering has two consequences: i) it leads to a loss of positive charge in the center, in conjunction with a gain in the edge region, and therefore gives raise to an electrostatic potential structure across the layer; ii) since the ion scattering is asymmetric in v_y (particles with smaller v_y are preferentially scattered) a significant velocity shear is induced at the edge of the current sheets [17] that induce a KHI [18].

The electron flow velocity can be approximated as

$$V_{ey} \approx U_e - \frac{c}{B_x}\frac{\partial \phi}{\partial z} \tag{4}$$

where the first term is the equilibrium flow velocity, the second term is the $\mathbf{E} \times \mathbf{B}$ velocity induced by the electrostatic potential, the inertia terms are neglected, and the equilibrium distribution are used to evaluate the pressure tensor. As it is shown in Fig. 4, the agreement between the velocity evaluated from Eq. 4 and the actual velocity resulting from NPIC simulation is remarkable at early stage of the current sheet evolution, before the current sheet profile strongly deviates from its initial shape.

Electron anisotropy is closely related to the plasma sheet structure. Anisotropic heating can be explained considering that for the case of noncrossing electrons with helical trajectories, the magnetic moment $\mu = mv_\perp^2/(2B_x)$ is an adiabatic invariant, since the time scales of the evolution of the system are slow compared to the typical electron scales. This implies that the perpendicular temperature is related to the local magnetic field

$$\frac{T_{e\perp}(z,t)}{T_{e\perp}(z,t=0)} \approx \frac{B_x(z,t)}{B_x(z,t=0)} \tag{5}$$

Where the electron orbits are helical, this expression provides a good estimate of the perpendicular heating at early stage of the current sheet evolution, as shown in Fig. 5. In the central region, the electron trajectories undergo a variety of complicated crossing orbits, and μ is no longer the relevant adiabatic invariant. (The comparison is less good in the thickest case, probably because of the numerical heating affecting this simulation.)

V. EFFECT OF LHDI ON THE TEARING INSTABILITY

We focus the attention on the effect of the nonlinear consequences of the LHDI on the tearing mode, in the case $\rho_i/L = 1.828$. In two-dimensional simulations without an initial perturbation, linear analysis and simulations give the same growth rate for the fastest growing tearing mode, $\gamma = 0.176\Omega_{ci}$, but tearing saturates at such a low amplitude that only a thin reconnected region results. The half-width, $w \approx 0.46L$ at $t\Omega_{ci} = 83$, should be compared with GEM challenge with a large initial perturbation, which covers the whole domain, $w \approx 10L$ at $t\Omega_{ci} \approx 30$ [14].

Nonlinear theories (e.g., see Refs. [37–39]) predict that anisotropic heating of electrons

during the growth of the instability reduces $T_{e\perp}/T_{e||}$) below 1, which strongly stabilizes tearing. Two-dimensional simulations performed by NPIC and CELESTE3D confirm the prediction and show that by $t\Omega_{ci} = 80$, $T_{e\perp}/T_{e||}$ is reduced from 1 to the range $0.83 - 0.87$, for which the linear code predicts that the maximum growth rate, $\gamma = 0.04\Omega_{ci}$, is a fraction of its initial value [14]. Perhaps small islands eventually coalesce into larger islands [40], but too slowly to account for the rapid reconnection observed in simulations extended in the third dimension [14].

It should be remarked that the Weibel instability may help to isotropize the electrons, but its growth rate is too small to influence the basic scenario of reconnection described here [40].

The LHDI also heats electrons anisotropically, but by contrast with the tearing instability, it increases rather than decreases $T_{e\perp}/T_{e||}$. The linear growth rates of the tearing instability obtained by the linear Vlasov code, Fig. 6, increases with $T_{e\perp}/T_{e||}$: for $T_{e\perp}/T_{e||} = 2$ the maximum growth rate, $\gamma \approx 3.8\Omega_{ci}$, is more than an order of magnitude larger than the maximum growth rate, $\gamma \approx 0.18\Omega_{ci}$, for $T_{e\perp}/T_{e||} = 1$. The wavelength of the fastest growing tearing mode decreases with increasing anisotropy: in the case $T_{e\perp}/T_{e||} = 2$ the maximum occurs for $k_x L = 2.25$, considerably larger that the typical $k_x L = 0.5$ seen for isotropic electrons. These results are consistent with earlier analysis [41–46] .

Since the anisotropic heating due to the LHDI occurs more rapidly than tearing growth, we consider simulations with an anisotropic electron temperature as an initial condition. With $T_{e\perp}/T_{e||} > 1$, NPIC and CELESTE3D simulations show that short wavelength modes grow to form small islands, which then merge to form a single large island (the dominant mode number $m_x = 1$ covers the whole domain by $t\Omega_{ci} \approx 20$). The reconnected flux is shown in Fig. 7. For $T_{e||}/T_{e\perp}$ between 1.5 and 2, reconnection involves the whole domain and the growth of the tearing instability does not saturate until all of the available magnetic flux is reconnected, similarly to the GEM challenge. Consistent with earlier results, the ratio $T_{e\perp}/T_{e||}$ decreases to ≈ 0.8 due to tearing, but then increases with the onset of fast reconnection [14].

Our results and others (see Refs. [12, 13]) show that thinner current sheets and higher current densities also enhance the linear growth rate and non-linear evolution of the tearing instability. The linear growth rate, Fig. 8, is higher for thinner current sheets: $\gamma = 0.176\Omega_{ci}$

for $\rho_i/L = 1.828$ (GEM challenge thickness) compared with $\gamma = 0.632\Omega_{ci}$ for $\rho_i/L = 3.656$. The wavelength of the fastest growing mode, however, is the same in all cases. For sufficiently thin current sheets, the tearing mode does not saturate at low levels, and covers the whole domain. The reconnected flux increases until it exhausts the supply by $t\Omega_{ci} \approx 20$ [14].

VI. CONCLUSIONS

The evolution of the LHDI and its influence on reconnection is studied using results from a linear kinetic code and two PIC codes employing very different algorithms: NPIC is a massively parallel explicit code and CELESTE3D is a implicit-moment method PIC code. The results of all the codes complement and confirm each other.

LHDI produces strong changes in the current profile. Depending on the current sheet thickness, current peaking or current bifurcation are observed. The changes in the current profile decreases with the thickness of the current sheet. Moreover, LHDI causes anisotropic heating of electrons. Also anisotropic heating decreases with the thickness of the current sheet.

The effects of the LHDI can be explained with a simple physical model. The nonlinear evolution of the LHDI give rise to a resonant scattering of ions into the noncrossing region of space. This in turn produces an electrostatic potential structure across the sheet leading to a strong change of the current density profile and perpendicular heating.

It is shown that both current peaking and anisotropic heating of the current sheet are effective in enhancing the linear growth rate of tearing instability. With a favorable anisotropy and a thin enough current sheet, the tearing instability grows large enough to decouple electrons and ions and reconnection can encompass the whole domain. The scaling study indicates that the effect of the LHDI is reduced with the thickness of the current sheet: when current sheet becomes thin enough, LHDI causes a strong peaking of the current profile and anisotropic electron heating. Both these effects are able to trigger the onset of reconnection.

It should be remarked that the the approach followed in the present study consider an isotropic and single peaked equilibrium, like the Harris current sheet, that is affected by the LHDI. The LHDI modifies the current profile and makes the electron anisotropic: the same relation between current sheet profiles and anisotropic electron distribution has been

pointed out in the study of current sheet equilibria. Within the Grad-Shafranov theory [47] and the Vlasov theory [33, 48], it has been shown that an anisotropic electron distribution ($T_{e\perp} > T_{e||}$) leads to a bifurcated current profile.

In the current sheets considered there is no background plasma, the guide field is not present, and no normal component of the magnetic field is introduced. The influence of these on reconnection onset needs further investigations.

VII. ACKNOWLEDGMENTS

The authors gratefully acknowledge useful discussions with B. Coppi, I. Furno, J. Huba, and B. Rogers.

This research is supported by the LDRD program at the Los Alamos National Laboratory, by the United States Department of Energy, under Contract no. W-7405-ENG-36 and by NASA, under the "Sun Earth Connection Theory Program" and the "Geospace Sciences Program."

[1] D. Biskamp, *Magnetic Reconnection in Plasmas* (Cambridge University Press, Cambridge, 2000).

[2] N.A. Krall and P.C. Liewer, Phys. Rev. A **4**, 2094 (1971).

[3] R.C. Davidson, N.T. Gladd, and C. Wu, Phys. Fluids **20**, 301 (1977).

[4] W. Daughton, Phys. Plasmas **10**, 3103 (2003).

[5] R.C. Davidson and N.T. Gladd, Phys. Fluids **18**, 1327 (1975).

[6] J.D. Huba, N.T. Gladd, and K. Papadopulos, Geophys. Res. Lett. **4**, 125 (1977).

[7] I. Shinohara, T. Nagai, M. Fujimoto *et al*, J. Geophys. Res. [Space Phys.] **103**, 20365 (1998).

[8] S. Bale, F. Mozer, and T. Phan. Geophys. Res. Lett. **29**, 2180 (2002).

[9] J.U. Brackbill, D.W. Forslund, K.B. Quest, and D. Winske, Phys. Fluids **27**, 2682 (1984).

[10] T. Carter, J. Ji, F. Trintchouk, M. Yamada, and R. Kulsrud, Phys. Rev. Lett. **88**, 015001 (2002).

[11] J.D. Huba, J.F. Drake, and N.T. Gladd, Phys. Fluids **23**, 552 (1980).

[12] M. Sholer, I. Sidorenko, C.H. Jaroschek *et al.*, Phys. Plasmas **10**, 3521 (2003).

[13] I. Shinohara and M. Fujimoto, Phys. Rev. Lett. (submitted).

[14] P. Ricci, J.U. Brackbill, W. Daughton, and G. Lapenta, Phys. Plasmas **11**, 4489 (2004).

[15] W. Daughton, G. Lapenta, and P. Ricci, Phys. Rev. Lett. **93**, 105004 (2004).

[16] G. Lapenta, J.U. Brackbill and W. Daughton. Phys. Plasmas **10**, 1577 (2003).

[17] W. Daughton, Phys. Plasmas **9**, 3668 (2002).

[18] G. Lapenta and J.U. Brackbill, Phys. Plasmas **9**, 1594 (2002).

[19] J. Birn, J.F. Drake, M.A. Shay, *et al.*, J. Geophys. Res. **106**, 3715 (2001).

[20] E.G. Harris, Nuovo Cimento **23**, 115 (1962).

[21] W. Daughton, Phys. Plasmas **6**, 1329 (1999).

[22] R. Morse and C. Nielson, Phys. Fluids **14**, 830 (1971).

[23] D. Forslund, Space Sci. Rev. **42**, 3 (1985).

[24] J.U. Brackbill and D.W. Forslund, in *Multiple Times Scales*, edited by J.U. Brackbill amd B.I. Cohen (Academic Press, Orlando, 1985), p. 271.

[25] H.X. Vu and J.U. Brackbill, Comput. Phys. Commun. **69**, 253 (1992).

[26] P. Ricci, G. Lapenta, and J.U. Brackbill, J. Comput. Phys. **183**, 117 (2002).

[27] R. Horiuchi and T. Sato, Phys. Plasmas **6**, 4565 (1999).

[28] P. Ricci, G. Lapenta, and J.U. Brackbill, Geophys. Res. Lett. **31**, L06901 (2004).

[29] R. Nakamura, W. Baumjohann, A. Runov *et al.*, Thin current sheets measured by Cluster at 250 Km tetrahedtron scale, The second workshop on thin current sheets, April 19-21, 2004, College Park MD, USA
(*http* : *//www.glue.umd.edu/ sitnov/TCS/tcs*_1_*files/ONLINE/TCS_Cluster*_2_*RN.pdf*)

[30] V.A. Sergeev, A. Runov, W. Baumjohann *et al.*, Geophys. Res. Lett. **30**, 1327 (2003).

[31] A. Runov, R. Nakamura, W. Baumjohann *et al.*, Geophys. Res. Lett. **30**, 1036 (2003).

[32] Y. Ren *et al.*, Bull. Am. Phys. Soc., 48, No. 7, p. 154, 2003, presentation #GP102.

[33] M.I. Sitnov, M. Swisdack, J.F. Drake, and P.N. Guzdar, Geophys. Res. Lett. **31**, L09805 (2004).

[34] H. Karimabadi, P.L. Pritchett, W. Daughton *et al.*, J. Geophys. Res. **108** (A11), 1401 (2003).

[35] M.A. Shay, J.F. Drake, R.E. Denton, and D. Biskamp, J. Geophys. Res. **103**, 9165 (1998).

[36] M. Swisdack, J.F. Drake, J.G. McIlhargey, and M.A. Shay, The transition from anti-parallel to component magnetic reconnection, J. Geophys. Res. (submitted).

[37] D. Biskamp, R.Z. Sagdeev, K. Shindler, Cosmic Electrodynamics **1**, 297 (1970).

[38] J.F. Drake and Y.C. Lee, Phys. Rev. Lett. **39**, 453 (1977).

[39] M.M. Kuznetsova and L.M. Zelenyi, Plasma Phys. Contr. Fusion **32**, 1183 (1990).

[40] H. Karimabadi, W. Daughton, and K.B. Quest, Geophys. Res. Lett., **31**, L18801 10.1029/2004GL020791 (2004).

[41] B. Coppi, Astrophys. J. **273**, L101 (1983).

[42] J. Chen and P. Palmadesso, Phys. Fluids **27**, 1198 (1984).

[43] J. Chen and Y.C. Lee, Phys. Fluids **28**, 2137 (1985).

[44] D.V. Forslund and B. Coppi, Bull. Am. Phys. Soc. **13**, 306 (1968).

[45] J. Ambrosiano, L.C. Lee, and Z.F. Fu, J. Geophys. Res. **91**, 113 (1986).

[46] Y. Shi, L.C. Lee, and Z.F. Fu, J. Geophys. Res. **92**, 12171 (1987).

[47] S.W.H. Cowley, Planet Space Sci **26**, 1037 (1978).

[48] J. Birn, K. Shindler, and M. Hesse, J. Geophys. Res. **109**, A02217 (2004).

- **Fig. 1.** The evolution of the current density, J_y is shown from simulations in the (y, z) plane. The dotted lines represent the current profiles at $t = 0$ averaged along y. Profiles at $t\Omega_{ci} = 4$ are shown by a solid line (NPIC simulation) and a dashed line (CELESTE3D simulation) for the $\rho_i/L = 1.828$ case (a), at $t\Omega_{ci} = 8$ for the $\rho_i/L = 0.915$ case (b), and at $t\Omega_{ci} = 17$ for the $\rho_i/L = 0.457$ case (c). The other current sheet parameters are: $\omega_{pe}/\Omega_{ce} = 2.88$, $m_i/m_e = 180$, and $T_i/T_e = 5$.

- **Fig. 2.** The electron pressure ratios P_{ezz}/P_{exx} (solid line) and P_{eyy}/P_{exx} (dashed line) are averages along y and plotted at time $t\Omega_{ci} = 4$ for the $\rho_i/L = 1.828$ case (a), at $t\Omega_{ci} = 8$ for the $\rho_i/L = 0.915$ case (b), and at $t\Omega_{ci} = 17$ for the $\rho_i/L = 0.457$ case (c). The other current sheet parameters are: $\omega_{pe}/\Omega_{ce} = 2.88$, $m_i/m_e = 180$, and $T_i/T_e = 5$. The results are from the NPIC simulations.

- **Fig. 3.** Cross section of phase space (top) in the $v_z - v_y$ plane, illustrating a drifting Maxwellian ion distribution and the phase space boundary in Eq. (3) for two different spatial positions in the layer. The shaded region in the upper figure corresponds to the approximate phase velocity of the waves $\omega/k_y \approx U_i/2$, which are in the proper region to resonantly scatter crossing ions into the noncrossing region of phase space. This scattering process and the resulting charge accumulation is illustrated in the lower figure.

- **Fig. 4.** The y-averaged y-velocity profile is shown from the NPIC simulation (red line) and compared with the estimate of Eq. (4) (blue line). The 3 cases are $\rho_i/L = 1.828$ (top), $\rho_i/L = 0.915$ (middle), and $\rho_i/L = 0.457$ (bottom).

- **Fig. 5.** The y-averaged $T_{e\perp}/T_{e||}$ profile is shown from the NPIC simulation (red line) and compared with the estimate of Eq. (5) (blue line). The 3 cases are $\rho_i/L = 1.828$ (top), $\rho_i/L = 0.915$ (middle), and $\rho_i/L = 0.457$ (bottom).

- **Fig. 6.** The growth rate γ/Ω_{ci} of the tearing mode is plotted as a function of k_xL for $T_{e\perp}/T_{e||} = 0.9$ (dotted), $T_{e\perp}/T_{e||} = 1$ (solid), $T_{e\perp}/T_{e||} = 1.5$ (dashed), $T_{e\perp}/T_{e||} = 2$ (dash-dotted). The other current sheet parameters are: $\omega_{pe}/\Omega_{ce} = 2.88$, $m_i/m_e = 180$, $\rho_i/L = 1.828$, and $T_i/T_{e||} = 5$.

- **Fig. 7.** The change in the reconnected flux $\Delta\Psi$ with time is compared for NPIC (a) and CELESTE3D (b) simulations. The parameters of the current sheets are: $T_{e\perp}/T_{e||} = 1$ (solid), $T_{e\perp}/T_{e||} = 1.5$ (dotted), $T_{e\perp}/T_{e||} = 2$ (dashed), $\omega_{pe}/\Omega_{ce} = 2.88$, $m_i/m_e = 180$, $\rho_i/L = 1.828$, and $T_i/T_{e||} = 5$.

- **Fig. 8.** The growth rate γ/Ω_{ci} of the tearing mode as a function of $k_x L$ is plotted for the plasma parameters $\omega_{pe}/\Omega_{ce} = 2.88$, $m_i/m_e = 180$, $T_i/T_e = 5$, and different values of ρ_i/L.

Table I. Electron pressure anisotropy, $P_{e\perp}/P_{e||}$, at the center of the current sheet, for different thicknesses of the current sheet, at time $t\Omega_{ci} = 4$ ($\rho_i/L = 1.828$), $t\Omega_{ci} = 8$ ($\rho_i/L = 0.915$), and $t\Omega_{ci} = 17$ ($\rho_i/L = 0.457$).

	$\rho_i/L = 1.828$	$\rho_i/L = 0.915$	$\rho_i/L = 0.457$
NPIC	2.20	1.09	1.03
CELESTE3D	1.84	1.01	0.95

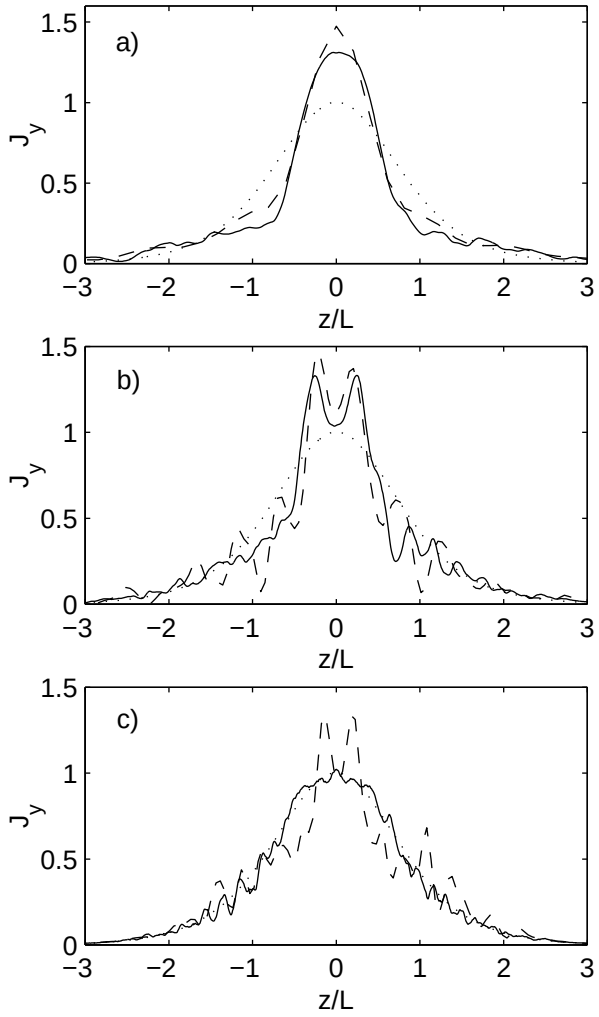
a)
b)
c)
J_y
z/L
0
0.5
1
1.5
−3
−2
−1
0
1
2
3

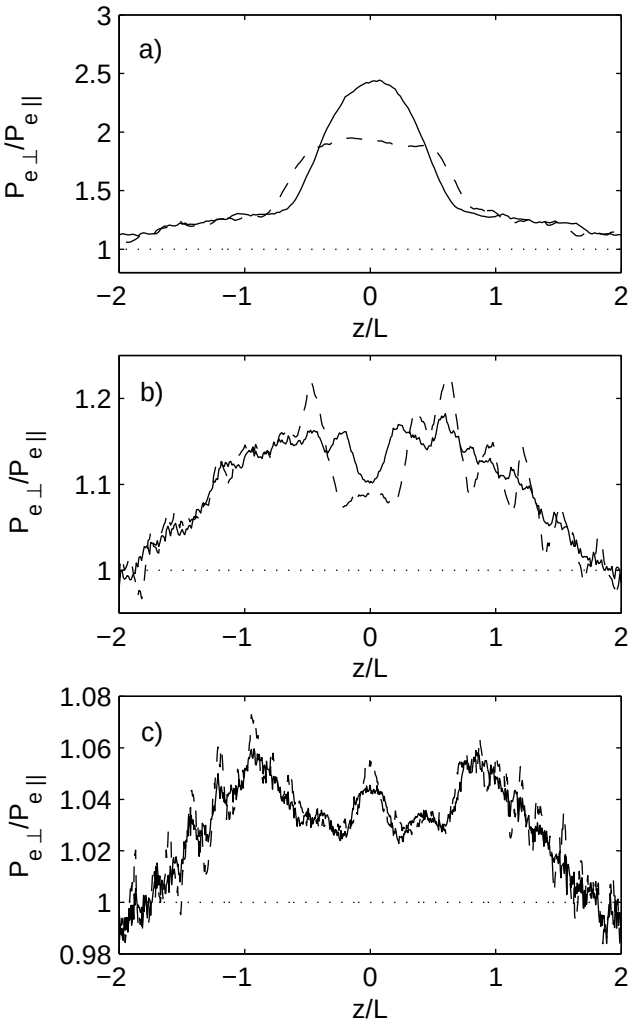
a)
b)
c)
$P_{e\perp}/P_{e\parallel}$
z/L
3
2.5
2
1.5
1
1.2
1.1
1.08
1.06
1.04
1.02
0.98
−2
−1
0
1
2

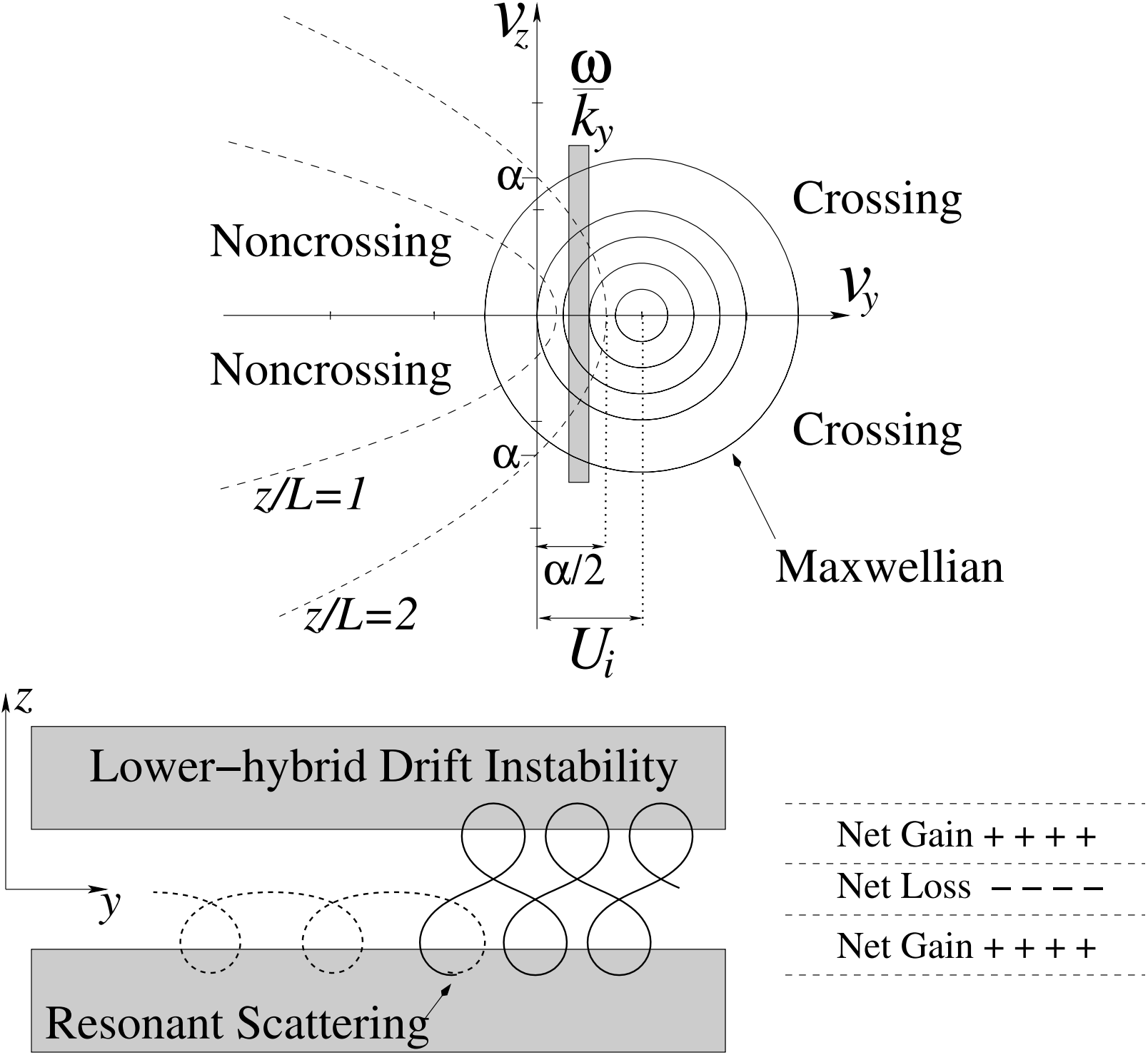
v_z
$\frac{\omega}{k_y}$
α
Noncrossing
Crossing
v_y
Noncrossing
Crossing
α
z/L=1
α/2
Maxwellian
z/L=2
U_i
z
Lower–hybrid Drift Instability
y
Resonant Scattering
Net Gain + + + +
Net Loss – – – –
Net Gain + + + +

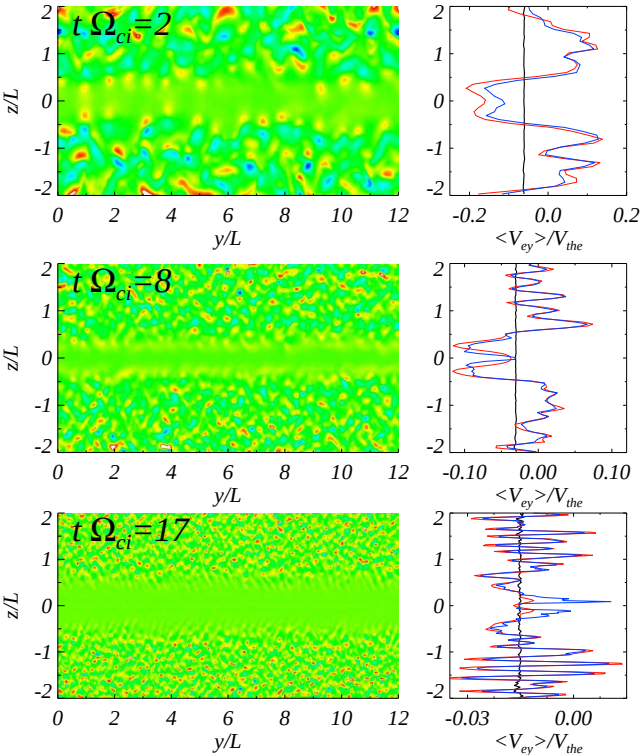
t Ω_ci=2
t Ω_ci=8
t Ω_ci=17
z/L
y/L
<V_ey>/V_the
2
1
0
-1
-2
0
2
4
6
8
10
12
-0.2
0.0
0.2
-0.10
0.00
0.10
-0.03
0.00

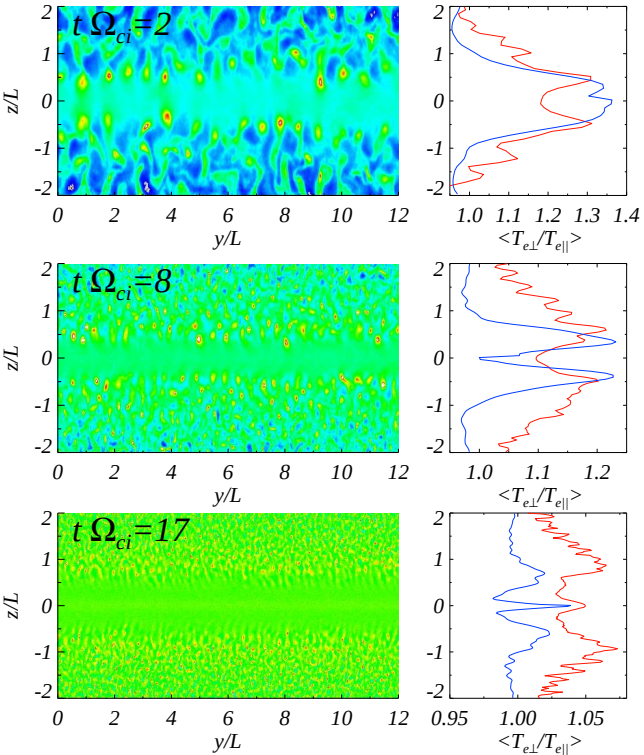
t Ω_ci=2
t Ω_ci=8
t Ω_ci=17
z/L
y/L
<T_e⊥/T_e||>
2
1
0
-1
-2
0
2
4
6
8
10
12
1.0
1.1
1.2
1.3
1.4
0.95
1.00
1.05

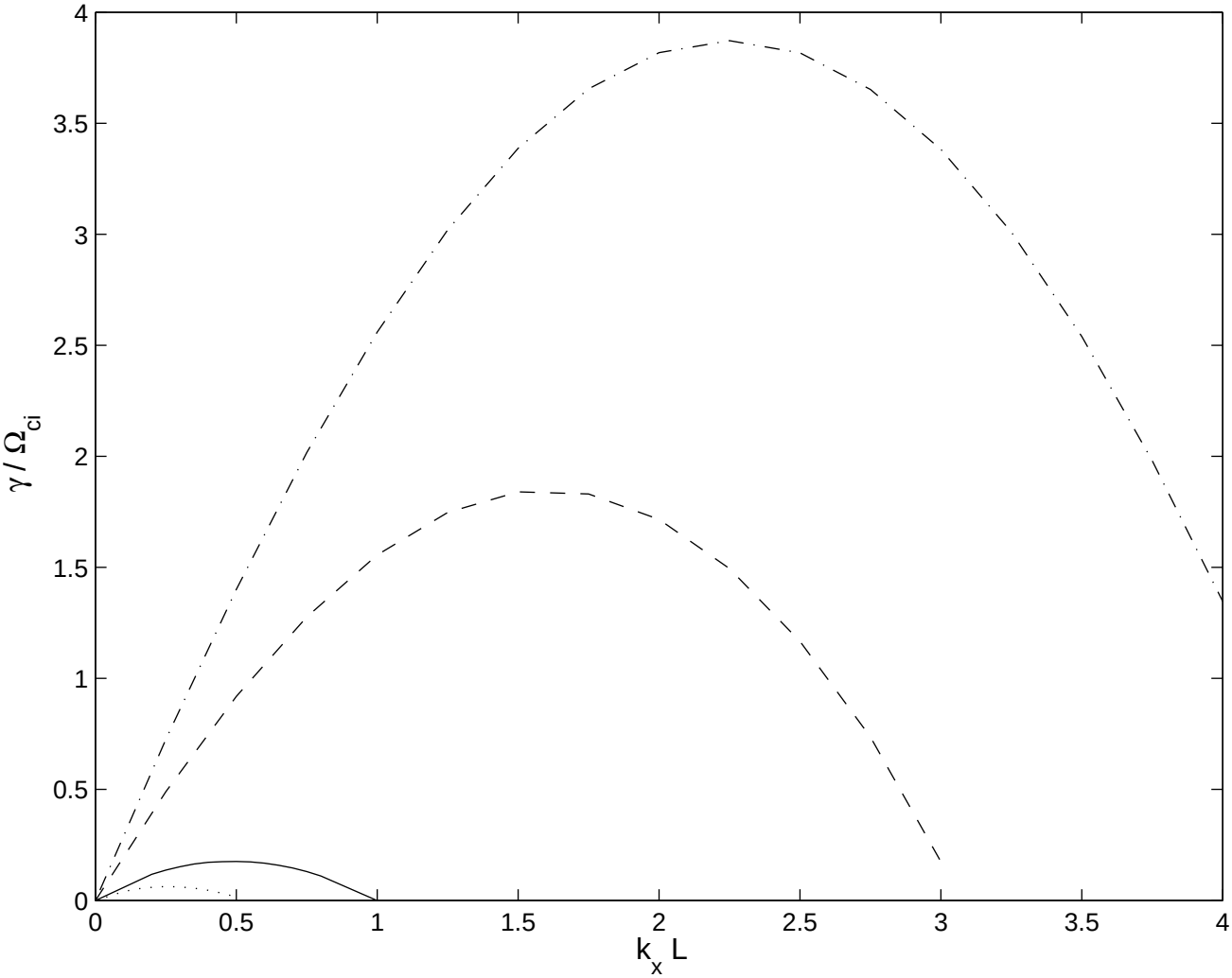
γ / Ω_ci
k_x L
0
0.5
1
1.5
2
2.5
3
3.5
4

a)

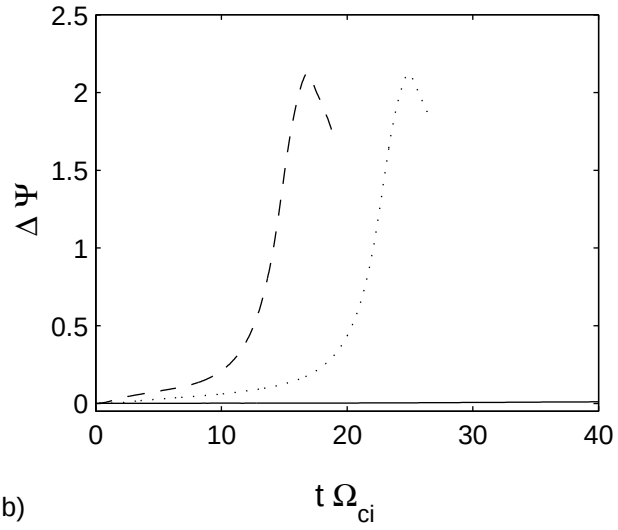

b)

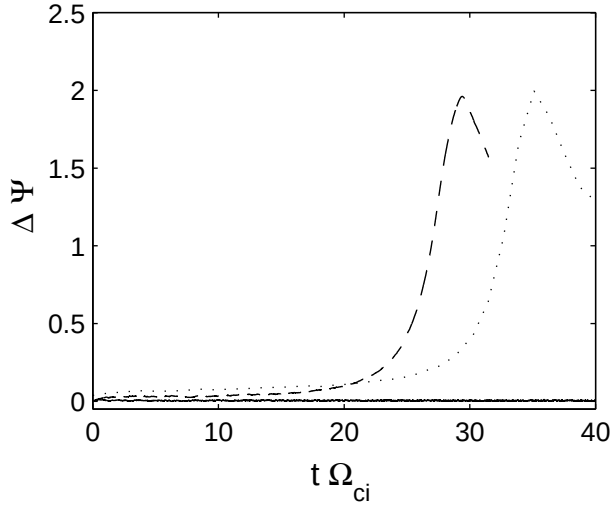

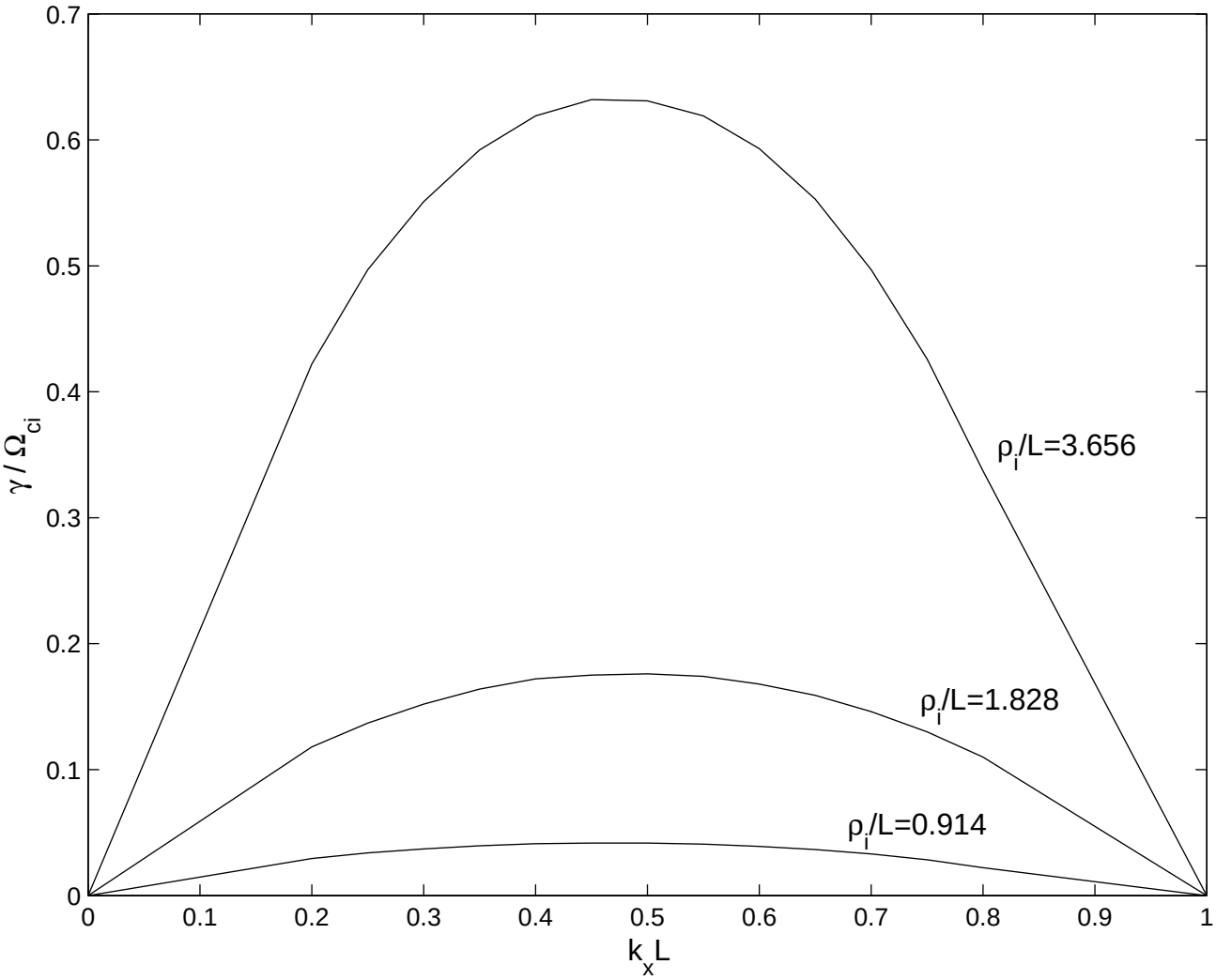
0.7
0.6
0.5
0.4
0.3
0.2
0.1
0
γ / Ω_ci
0
0.1
0.2
0.3
0.4
0.5
0.6
0.7
0.8
0.9
1
k_x L
ρ_i/L=3.656
ρ_i/L=1.828
ρ_i/L=0.914